Physica A 391 (2012) 3607–3615

Contents lists available at SciVerse ScienceDirect

Physica A

journal homepage: www.elsevier.com/locate/physa

Scaling dynamics for a particle in a time-dependent potential well

Diogo Ricardo da Costa, Mário Roberto Silva, Juliano A. de Oliveira, Edson D. Leonel *

Departamento de Estatística, Matemática Aplicada e Computação, UNESP, Univ Estadual Paulista Av.24A, 1515, CEP: 13506-900, Rio Claro, SP, Brazil

ARTICLE INFO

Article history:
Received 1 February 2012
Available online 15 February 2012

Keywords:
Scaling
Chaos

ABSTRACT

Some dynamical properties for a classical particle confined in an infinitely deep box of potential containing a periodically oscillating square well are studied. The dynamics of the system is described by using a two-dimensional non-linear area-preserving map for the variables energy and time. The phase space is mixed and the chaotic sea is described using scaling arguments. Scaling exponents are obtained as a function of all the control parameters, extending the previous results obtained in the literature.

1. Introduction

Dynamical systems described by mappings have been considered widely during the past years [1,2]. In particular, and for the most simple case, i.e., for a system with 1 and 1/2 degrees of freedom, which corresponds to a time perturbation in a system with one degree of freedom, the description of Hamiltonian systems leads many times to two-dimensional non-linear area-preserving mappings. Many different applications of the formalism using area-preserving mappings are observed, in particular, studying magnetic field lines in toroidal plasma devices with reversed shear (such as tokamaks) [3–6], waveguide [7–11], Fermi acceleration [12], billiards [13–15] and many other generalizations [16–19].

In this paper we consider some dynamical properties of a problem with 1 and 1/2 degrees of freedom. The model consists of a classical particle confined inside an infinitely deep potential well and contains a time periodically moving square well. The Hamiltonian describing the model is $H(x, p, t) = p^2/(2m) + V(x, t)$, where $V(x, t) = V_0(x) + V_1(x, t)$, where x, p and t correspond to the position, momentum coordinates and time, respectively. The potential $V_0(x)$ denotes the integrable part of the Hamiltonian while $V_1(x, t)$ leads to the non-integrable part. As will be shown in the next section, the potential $V_1(x, t)$ is controlled by three relevant control parameters. If they are changed accordingly, a phase transition from integrability to non-integrability is observed. Among other things we discuss in the paper, this transition is basically the main focus of the present work and extends the results obtained previously in Ref. [20].

The dynamics of the model is described in terms of a two-dimensional non-linear area-preserving mapping for the variables energy and time. The phase space is mixed in the sense that periodic islands are observed surrounded by a chaotic sea characterised by a positive Lyapunov exponent. The *size* of the chaotic sea depends on the control parameters and is limited by a set of invariant tori (also called invariant spanning curves) that prevents the unlimited energy of the particle (also known as Fermi acceleration). If the law which controls the time perturbation of the moving well is smooth enough, Fermi acceleration [21] is not observed (see Ref. [22] for a similar discussion in one-dimensional Fermi accelerator models and Ref. [23] where it occurs for specific ranges of control parameters).

The *size* of the chaotic sea and, consequently, the position of the first invariant spanning curve bordering the chaotic sea are strongly dependent on the control parameters of the model. Therefore, the average properties of the chaotic sea can be described by using scaling formalism and scaling exponents can be obtained, in particular considering the behaviour of

* Corresponding author.
E-mail address: edleonel@rc.unesp.br (E.D. Leonel).

0378-4371/
doi:10.1016/j.physa.2012.02.011

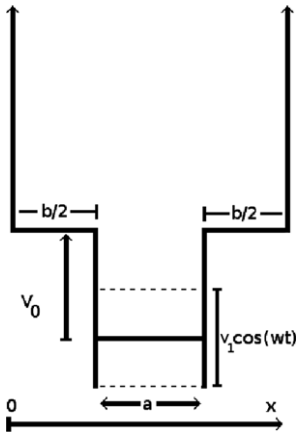

Fig. 1. Sketch of the potential considered.

the average energy of the particle or the average standard deviation of the energy. Then, classes of universality [24] can be defined according to the numerical values of the scaling exponents.

This paper is organised as follows. In Section 2, we describe the model under consideration and four different potential shapes which lead to the same characterisation of the problem. Our numerical results and the scaling exponents are shown in Section 3, together with a discussion about the behaviour of the Lyapunov exponents. Final remarks and conclusions are drawn in Section 4.

2. The model and the map

In this section we discuss the model and the corresponding map that describes the dynamics of the system. The model consists of a classical particle confined inside a box of an infinitely deep potential and contains an oscillating square well in the middle. We assume that the oscillations of the bottom are periodic in time and are given by a cosine function. A typical sketch of the potential is shown in Fig. 1. Along region b (where the potential is constant and equal to V_0) and region a (where potential is time dependent), the velocity of the particle is constant because no dissipative forces act on the particle. The total energy is obtained by the summation of the kinetic and potential energies. The motion of the particle changing from one region to another is marked by an abrupt change in its kinetic energy.

We emphasise that different kinds of potential shape lead to similar dynamics. For a chain of infinitely many and symmetric oscillating square wells with their bottoms moving periodically and synchronised in time (see Ref. [25] and in Fig. 2(a)), the dynamics leads to diffusion in space. One can also assume a single oscillating square well with periodic boundary conditions, as shown in Fig. 2(b). Finally, a step potential whose bottom moves periodically in time confined in an infinite box of potential (see Fig. 2(c)) leads to similar results in the phase space.

In this paper we consider the potential as shown in Fig. 1, and is given by

$$V(x,t) = \begin{cases} \infty, & \text{if } x \le 0 \text{ or } x \ge (a+b) \\ V_0, & \text{if } 0 < x < \dfrac{b}{2} \text{ or } \left(a+\dfrac{b}{2}\right) < x < (a+b) \\ V_1\cos(\omega t), & \text{if } \dfrac{b}{2} \le x \le \left(a+\dfrac{b}{2}\right), \end{cases} \tag{1}$$

where the control parameters a, b, V_0, V_1 and ω are constants. Considering the symmetry of the problem, the mapping is obtained upon the entrance of the particle in the oscillating square well. To construct the map, we suppose that at the time $t = t_n$, the particle has energy $E = E_n$ and is ready to enter the oscillating square well. After entering the well, it experiences an abrupt change in its kinetic energy, leading to $K_n{}' = E_n - V_1\cos(\omega t_n) = \frac{1}{2}m{v_n}'^2$, where $|v_n'| = \sqrt{2K_n'/m}$ is constant. Arriving on the other side of the well the energy of the particle is $E_n{}' = K_n{}' + V_1\cos[\omega(t_n + \Delta t_n')]$, where $\Delta t_n' = a/|v_n'|$. If the particle does not have enough energy to escape the well it is reflected backwards, given that $E_n' \le V_0$. It may experience many other successive reflections until it escapes the well and E_n' may be redefined more generically as $E_n{}' = K_n{}' + V_1\cos[\omega(t_n + i\Delta t_n')]$, where i is the smallest positive integer number that matches the condition $E_n{}' > V_0$, a condition which assures the escape of the particle. Once the particle escapes the oscillating well it travels towards the infinite potential boundary of the box, experiences an elastic reflection from it and moves backwards towards a next entrance of the oscillating square well. The new energy of the particle is given by $E_{n+1} = E_n + V_1\{\cos[\omega(t_n + i\Delta t_n')] - \cos(\omega t_n)\}$. The time at the next entrance is written as $t_{n+1} = t_n + i\Delta t_n{}' + \Delta t_n{}''$, where $\Delta t_n'' = b/|v_n''|$ with $|v_n|'' = \sqrt{2K_n{}''/m}$ and $K_n'' = E_{n+1} - V_0$.

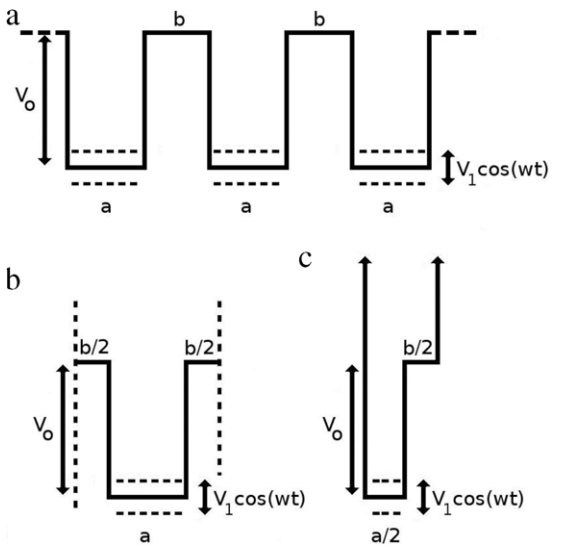

Fig. 2. (a) A chain of infinitely many and symmetric oscillating square wells with their bottoms moving periodically and synchronised in time. (b) A single oscillating square well. (c) A step potential whose bottom moves periodically in time.

As one can see, there are many control parameters which are not relevant to describe the dynamics; five in total, namely a, b, V_0, V_1 and ω. So, it is convenient to define some dimensionless variables such as $\delta = V_1/V_0$, $r = b/a$, $e_n = E_n/V_0$, $N_c = \omega/(2\pi)\ (a/\sqrt{2V_0/m})$ and the time is measured in terms of the number of oscillations of the moving well, $\phi = \omega t$. The parameter N_c corresponds to the number of oscillations that the square well completes in time $t = a/\sqrt{2V_0/m}$.

With this set of new variables, the mapping which describes the dynamics of the system is written as

$$T: \begin{cases} e_{n+1} = e_n + \delta[\cos(\phi_n + i\Delta\phi_a) - \cos\phi_n] \\ \phi_{n+1} = [\phi_n + i\Delta\phi_a + \Delta\phi_b](\mathrm{mod}\ 2\pi), \end{cases} \tag{2}$$

where the auxiliary variables are given by

$$\Delta\phi_a = \frac{2\pi N_c}{\sqrt{e_n - \delta\cos(\phi_n)}}, \qquad \Delta\phi_b = \frac{2\pi N_c r}{\sqrt{e_{n+1} - 1}}.$$

During the dynamics, when the particle stays confined in the oscillating square well with its energy at the boundaries $1-\delta < e \leq 1$, a trapping would be longer or not. The distribution of successive reflection numbers obeys a power law with exponent around -3, as shown in Fig. 3.

Given the determinant of the Jacobian matrix is equal to the unity, the mapping (2) is area preserving. The phase space of the model is mixed, containing periodic islands, chaotic sea and a set of invariant spanning curves, as one can see in Fig. 4.

Once the equations of the mapping are given, the corresponding fixed points can be obtained. The fixed points of period one, without multiple reflections, are obtained by the condition $e_{n+1} = e_n = e^*$ and $\phi_{n+1} = \phi_n + 2m\pi = \phi^*$, where m is a non-negative integer number. Considering the periodic functions of the mapping it is necessary to apply two different procedures to obtain the fixed points $[e^*, \phi^*]$: (i) obtained analytically by the expressions

$$\left[\left(\frac{N_c r}{m-k}\right)^2 + 1, \arccos\left(\frac{1}{\delta}\left(e - \left(\frac{N_c}{k}\right)^2\right)\right)\right], \tag{3}$$

and

$$\left[\left(\frac{N_c r}{m-k}\right)^2 + 1, 2\pi - \arccos\left(\frac{1}{\delta}\left(e - \left(\frac{N_c}{k}\right)^2\right)\right)\right]; \tag{4}$$

where k arises from the condition that the arguments of the periodic cosine function must differ from each other by integer multiples of 2π, then $\Delta\phi_a = k2\pi$. The other possibility is $\Delta\phi_a = k2\pi - 2\phi^*$, leading to the procedure (ii) which gives the fixed points after a numerical solution of

$$1 + \left(\frac{\pi N_c r}{\pi(m-k) + \phi}\right)^2 - \delta\cos(\phi) - \left(\frac{\pi N_c}{\pi k - \phi}\right)^2 = 0, \tag{5}$$

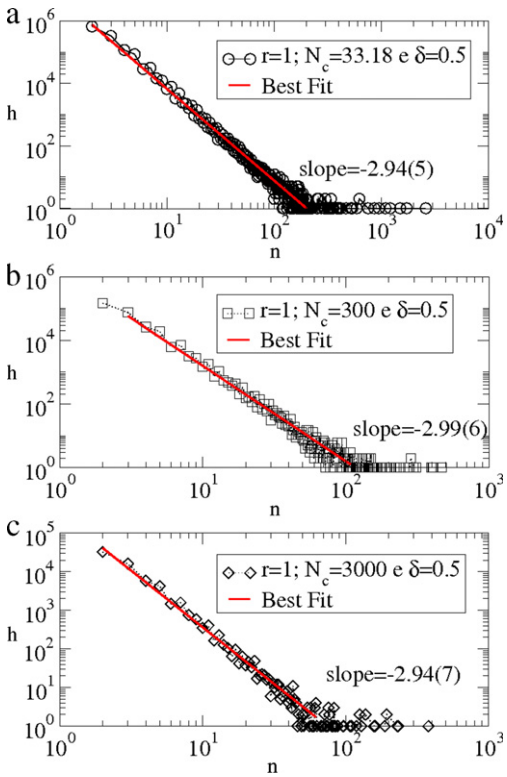

Fig. 3. (Colour online) Distribution of successive reflections of the particle by the oscillating square well. The control parameters used were $r = 1, \delta = 0.5$ and: (a) $N_c = 33.18$; (b) $N_c = 300$ and (c) $N_c = 3000$.

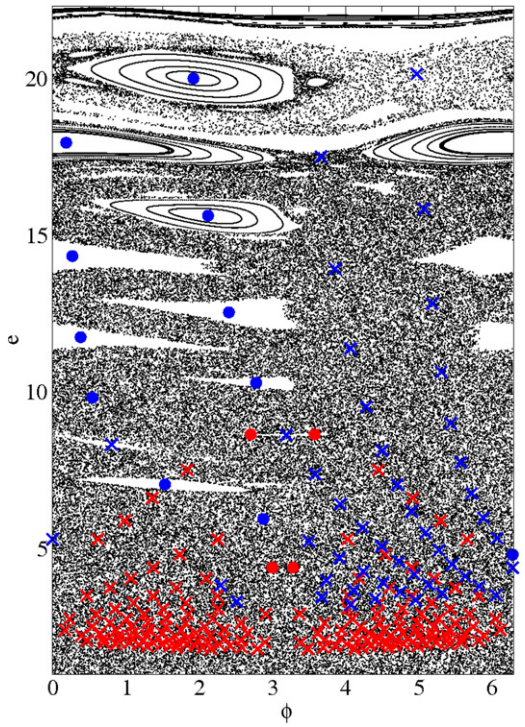

Fig. 4. (Colour online) Phase space for the mapping (2). The circles correspond to elliptic fixed points while crosses denote hyperbolic ones. The red (grey) colour is used to identify treatment (i) and blue (black) colour to treatment (ii) (see details in the text). The control parameters used were $r = 1, N_c = 33.18$ and $\delta = 0.5$.

where $m > k$, with m and k integers larger than 1. Solution of Eq. (5) furnishes ϕ numerically. The corresponding energy is given by

$$e = \left(\frac{\pi N_c r}{\pi(m-k)+\phi}\right)^2 + 1. \tag{6}$$

The characterisation of the fixed points is made by the eigenvalues of the Jacobian matrix J [26]. If the evaluation of the eigenvalues at the fixed point produces $(\mathrm{Tr}J)^2 > 4$, the fixed point is said to be hyperbolic. On the other hand, for the case of $(\mathrm{Tr}J)^2 < 4$, the fixed points are classified as elliptic. The fixed points for mapping (2) are identified in Fig. 4 by circles (elliptic fixed point) and crosses (hyperbolic fixed point). The red (grey) circles (crosses) correspond to elliptic (hyperbolic) fixed points obtained by Eqs. (3) and (4) while the blue (black) are obtained via Eqs. (5) and (6).

3. Numerical results

Let us now discuss the numerical results. We start by presenting the Lyapunov exponents characterising the chaotic sea below the first invariant spanning curve. It is known that Lyapunov exponents are used in order to verify if the system is chaotic or not. Basically, the procedure to obtain the Lyapunov exponents consists of verifying if two trajectories, initially close to each other, will diverge exponentially for an infinitely long time. According to Ref. [27], the Lyapunov exponents can be obtained by

$$\lambda_j = \lim_{n\to\infty} \frac{1}{n} \ln |\Lambda_j^{(n)}|, \quad j = 1, 2 \tag{7}$$

where $\Lambda_j^{(n)}$ are the eigenvalues of the matrix $B = \prod_i^n J_i(e_i, \phi_i)$ and J_i is the Jacobian matrix of the system evaluated over the orbit. If the system exhibits at least one positive Lyapunov exponent, then it has chaotic components.

Fig. 5(a) shows the behaviour of the positive Lyapunov exponent as a function of n for six different initial conditions randomly chosen along the chaotic sea. The control parameters used were $r = 1$, $N_c = 500$ and $\delta = 0.5$. After an initial fluctuation, the positive Lyapunov exponent converges to a constant value for large enough n. Given the convergence, the average Lyapunov exponent can be obtained as $\bar{\lambda} = \frac{1}{6}\sum_{i=1}^{6} \lambda_i$, where each of the λ_i correspond to the asymptotic value of the Lyapunov exponent for the initial condition (e_i, ϕ_i) with $i = 1, 2, \ldots, 6$. After taking the average, the behaviour of $\bar{\lambda}$ is obtained as function of the control parameters N_c, δ and r. Fig. 5(b) shows a plot of $\bar{\lambda} \times N_c$ for fixed $r = 1$ and $\delta = 0.5$. As one can see, the positive Lyapunov exponent varies from $\bar{\lambda} \approx 0.5$ for $N_c = 1$ up to $\bar{\lambda} \approx 2$ for $N_c = 10^3$. It also has a monotonic tendency of growth as a function of N_c. Note, however, that increasing N_c corresponds to raising the number of oscillations of the well and consequently increasing the *randomness* of the system, leading to an increase in the Lyapunov exponent. A plot of $\bar{\lambda} \times \delta$ is shown in Fig. 5(c). The control parameters used were $r = 1$ and $N_c = 33.18$. Here, it is easy to see that small values of δ, which corresponds to small fluctuations of the oscillating square well, produce a large Lyapunov exponent. A minimum value of $\bar{\lambda} \approx 1.4$ was observed for $\delta \approx 0.2$. Finally, a plot of $\bar{\lambda} \times r$ is shown in Fig. 5(d) for fixed $\delta = 0.5$ and $N_c = 33.18$. Since the control parameter $r = b/a$, increasing r for a fixed N_c corresponds to increasing b, thus, increasing the distance from the well up to the box of potential. Such an increase leads to a long flight of the particle until the next entrance in the oscillating square well, yielding an increase of the number of oscillations of the moving well and consequently increasing the *randomness* of the system. The sudden jumps in the behaviour of the Lyapunov exponent are explained as the destruction of invariant spanning curves, leading to a joining of different chaotic regions (see Ref. [23] for a discussion in the Fermi–Ulam model and Ref. [28] for the time-dependent square well).

Let us now address properly the scaling description of the chaotic sea. The position of the first invariant spanning curve (invariant tori) bordering the chaotic sea depends on the control parameters. As they change, the position of the first invariant spanning curve varies, allowing the chaotic sea to enlarge or reduce. See Ref. [29] for a phenomenological description of the estimation of the position of the first invariant spanning curve for a family of 2-D area-preserving mapping with one of the variables diverging in the limit of vanishing action. Our main interest is to characterise the behaviour of the average energy and, hence, the average standard deviation of the energy for the chaotic sea as a function of the control parameters. To do so, we define the average energy as

$$\bar{e}(n, \delta, N_c, r) = \frac{1}{n}\sum_{i=1}^{n} e_i, \tag{8}$$

and the average standard deviation of the energy is given by

$$\omega(n, \delta, N_c, r) = \frac{1}{M}\sum_{j=1}^{M} \sqrt{\overline{e_j^2}(n, \delta, N_c, r) - \bar{e}_j^2(n, \delta, N_c, r)}, \tag{9}$$

where M denotes an ensemble of different initial conditions. Fig. 6 shows three different curves of ω, as a function of n, obtained for different values of the control parameter N_c. As one can see, after an initial and short transient, ω starts to grow according to a power law and eventually, after reaching a characteristic crossover time, n_x, it bends towards a regime of

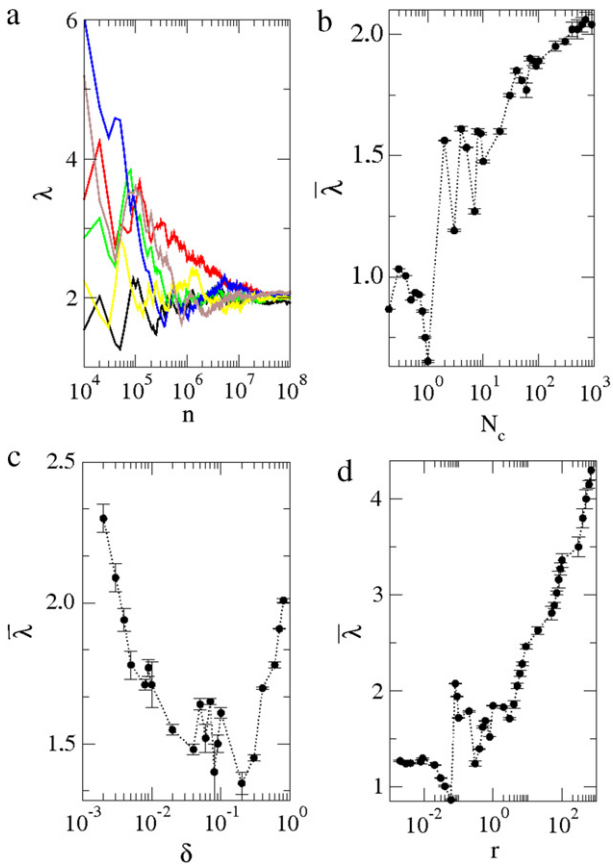

Fig. 5. (Colour online) (a) Time evolution of the positive Lyapunov exponent for six different initial conditions, evolved up to 5×10^8 times. The control parameters used were $r = 1$; $N_c = 500$ and $\delta = 0.5$. (b) Plot of $\bar{\lambda} \times N_c$ for fixed $r = 1$ and $\delta = 0.5$. (c) Plot of $\bar{\lambda} \times \delta$ for fixed $r = 1$ and $N_c = 33.18$. (d) Plot of $\bar{\lambda} \times r$ for fixed $N_c = 33.18$ and $\delta = 0.5$.

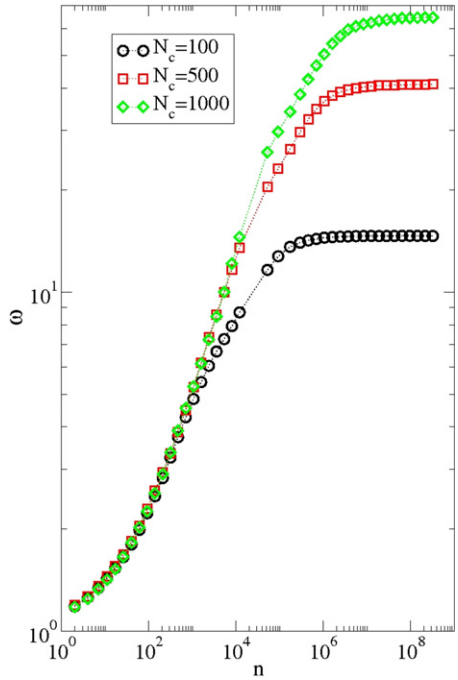

Fig. 6. (Colour online) Plot of $\omega \times n$ for fixed $r = 1$, $\delta = 0.5$ and three different N_c, namely $N_c = 100$, $N_c = 500$ and $N_c = 1000$.

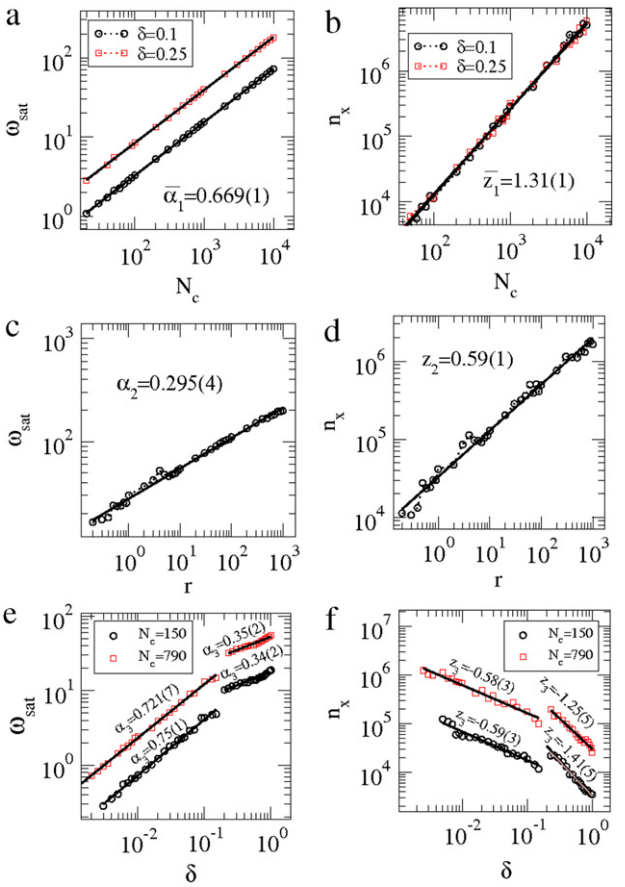

Fig. 7. (Colour online) Behaviour of (a) $\omega_{\text{sat}} \times N_c$ and (b) n_x as a function of N_c. The control parameters used were: black bullet $r = 1$ and $\delta = 0.1$; red bullet $r = 1$ and $\delta = 0.25$. (c) Plot of $\omega_{\text{sat}} \times r$; (d) n_x as a function of r. The parameters used were $\delta = 0.5$ and $N_c = 500$. (e) Plot of ω_{sat} as a function of δ and (f) $n_x \times \delta$. The control parameters used were $r = 1$, $N_c = 150$ and $N_c = 790$.

saturation for long enough n. Similar behaviour is observed when the control parameters δ and r are varied. Based on such a behaviour we propose the following scaling hypotheses:

- (i) For $n \ll n_x$, the behaviour of ω can be described as

$$\omega(n\delta^2, N_c, r, \delta) \propto [n\delta^2]^{\beta}, \tag{10}$$

  where β is the acceleration exponent;
- (ii) For $n \gg n_x$, ω_{sat} is given by

$$\omega_{\text{sat}}(n\delta^2, N_c, r, \delta) \propto {N_c}^{\alpha_1} r^{\alpha_2} \delta^{\alpha_3}, \tag{11}$$

  where α_i for $i = 1, 2, 3$ are the saturation exponents;
- (iii) The characteristic crossover n_x is written as

$$n_x(n\delta^2, N_c, r, \delta) \propto {N_c}^{z_1} r^{z_2} \delta^{z_3}, \tag{12}$$

  and z_i with $i = 1, 2, 3$ are the crossover exponents.

The saturation exponents α_i and the crossover exponents z_i can be found if the behaviour of ω_{sat} and n_x are obtained as functions of the control parameters. After some extensive numerical investigation they are shown in Fig. 7. Additionally, we found that the acceleration exponent is $\beta \cong 0.5$.

Applying a power-law fitting in Fig. 7(a, b) we obtain $\alpha_1 = 0.669(1)$ and $z_1 = 1.31(1)$. Extending the procedure to the variable r, as shown in Fig. 7(c, d), we obtain $\alpha_2 = 0.295(4)$ and $z_2 = 0.59(1)$. Finally, Fig. 7(e, f) shows the behaviour of ω_{sat} and n_x as a function of the control parameter δ. In the last case, we can see two different sets of values for α_3 and z_3. The explanation for such a difference is due to a sudden destruction of the invariant spanning curve that separates two different chaotic regions (see Ref. [23] for occurrence of such destruction in the Fermi–Ulam model). After the destruction and the joining of two chaotic components, the critical exponents change substantially. Before the destruction, say $\delta < 0.2$,

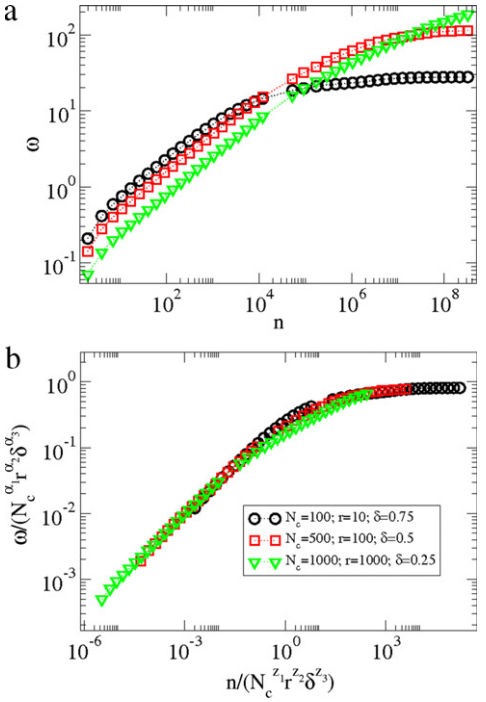

Fig. 8. (Colour online) (a) Behaviour of $\omega \times n$ for different values of the control parameters r, δ and N_c; (b) merger of all curves shown in (a) onto a single plot, after a suitable rescale of axis.

we obtain $\alpha_3 = 0.721(7)$ and $z_3 = -0.58(3)$ for $N_c = 790$ and $\alpha_3 = 0.75(1)$ and $z_3 = -0.59(3)$ for $N_c = 150$. On the other hand, after the destruction, i.e. for $\delta > 0.2$, the exponents obtained were $\alpha_3 = 0.35(2)$ and $z_3 = -1.25(5)$ for $N_c = 790$ and $\alpha_3 = 0.34(2)$ and $z_3 = -1.41(5)$ for $N_c = 150$. To check the validity of the scaling hypotheses we can rescale the axis properly and a single plot for different curves of ω is obtained, as shown in Fig. 8.

Let us discuss the classes of universality. We have to emphasise that the phase transition we are considering in this paper is not defined in the rigorous Statistical Mechanics point of view. The phase transition we consider is based on the fact that, for specific control parameters, the system is integrable, for example if $\delta = 0$ or $N_c = 0$, and non-integrable for the general case of $\delta \neq 0$, $N_c \neq 0$ and $r \neq 0$. Describing the behaviour of average quantities along the chaotic sea, in particular the average standard deviation of the energy, as a function of the control parameters has been used for a long time. Given the exponents are known, the system can be rescaled conveniently, which leads to all quantities be scaling independent. The set of scaling exponents obtained define to what class of universality the system belongs. To illustrate two cases we consider the following examples: (i) Fermi–Ulam model [30] and periodically corrugated waveguide [7,8]; (ii) a family of two-dimensional area-preserving mapping [31] and the present model studied.

For case (i) the Fermi–Ulam model (a classical particle confined and bouncing between two rigid walls; one of them is fixed and the other one is periodically time varying—collisions are elastic and no damping forces are present) is described via a two-dimensional non-linear, area-preserving mapping for the variables velocity of the particle and phase of the moving wall. The scaling exponents obtained for the average velocity along the chaotic sea were [30]: $\alpha = 0.5$, $\beta = 0.5$ and $z = -1$. The corrugated waveguide model, however, considers the description of a light beam moving inside two mirrors, of which one is flat and the other is periodically corrugated. The mapping describes the position of the light beam at each reflection with the mirror and the angle of the light beam trajectory [7,8], thus there is no velocity involved in this model. The critical exponents obtained were the same as those obtained for the Fermi–Ulam model. The models are totally independent of each other, but, near such a transition, the chaotic seas of both models have qualitatively the same general behaviour. Thus, the two models belong to the same class of universality near this transition.

For case (ii) a family of mapping is written as Ref. [31]

$$T: \begin{cases} x_{n+1} = \left[x_n + \dfrac{a}{y_{n+1}^{\gamma}} \right] \pmod 1 \\ y_{n+1} = |y_n - b \sin(2\pi x_n)|, \end{cases} \tag{13}$$

where a, b and γ are the control parameters. The determinant of the Jacobian matrix is $\det(J) = \text{sign}(y_n - b \sin(2\pi x_n))$, where $\text{sign}(u) = 1$ if $u > 0$ and $\text{sign}(u) = -1$ if $u < 0$. For $\gamma < 0$, depending on the initial conditions and control parameters, the unlimited growth of the average value of y, namely $\bar{y}$, can be observed. Such a growth happens since large values of y imply a large number of oscillations for the sine function. In the regime of very large oscillations, the sine function works more likely

as a random function, yielding an unlimited growth for $\bar{y}$. To avoid such a condition and confirm the existence of invariant tori, γ was considered in the range $0 < \gamma \leq 1$. The parameter a in mapping (13) corresponds to the control parameter N_c in mapping (2). Raising N_c corresponds to increasing the randomness of the model, a similar behaviour happens when a is raised in (13). Keeping fixed $\gamma = 1/2$ in mapping (13) leads to the corresponding square root in time for mapping (2), we obtained that the critical exponents are the same, within an uncertainty error. The two different models exhibit the same critical exponents and therefore belong to the same class of universality for such a phase transition considering the corresponding control parameter.

4. Summary and conclusions

We have studied the dynamics of a classical particle confined in a box of infinitely deep potential containing a periodically oscillating square well. We have shown that the two-dimensional area-preserving mapping that describes the dynamics of the model has three relevant control parameters. We have obtained the mapping that describes the dynamics of the system and shown that the phase space is mixed with a chaotic sea characterised by using the Lyapunov exponents. We have also studied some average properties of the chaotic sea below the first invariant spanning curve bordering the chaotic sea, using a scaling approach, as a function of all three control parameters. We have found the scaling exponents, namely, the acceleration exponent, the saturation exponent and the crossover exponent, and after a suitable rescaling of the axis, we have shown a collapse of all the curves of the average standard deviation of the energy onto a single plot. Such a kind of behaviour is typical of systems experiencing phase transition. In particular, we have considered the transition from integrability to non-integrability.

Acknowledgments

DRC and JAO acknowledge the Brazilian agency CNPq. EDL thanks the CNPq, FUNDUNESP and FAPESP, Brazilian agencies. This research was supported by resources supplied by the Center for Scientific Computing (NCC/GridUNESP) of the São Paulo State University (UNESP). The authors kindly thank Diego Fregolente Mendes de Oliveira for a careful reading of the paper.

References

[1] A.J. Lichtenberg, M.A. Lieberman, Regular and Chaotic Dynamics, in: Appl. Math. Sci., vol. 38, Springer-Verlag, New York, 1992.
[2] G.M. Zaslavsky, Physics of Chaos in Hamiltonian Systems, Imperial College Press, London, 1998.
[3] K. Ullmann, I.L. Caldas, Chaos Solitons Fractals 11 (2000) 2129.
[4] I.L. Caldas, J.M. Pereira, K. Ullmann, R.L. Viana, Chaos Solitons Fractals 7 (1996) 991.
[5] S.S. Abdullaev, G.M. Zaslavsky, Phys. Plasmas 3 (1996) 516.
[6] A. Punjabi, H. Ali, A. Boozer, Phys. Plasmas 4 (1997) 337.
[7] E.D. Leonel, Phys. Rev. Lett. 98 (2007) 114102.
[8] A.F. Rabelo, E.D. Leonel, Braz. J. Phys. 38 (2008).
[9] A.L. Virovlyansky, G.M. Zaslavsky, Chaos 10 (2000) 211.
[10] I.P. Smirnov, A.L. Virovlyansky, G.M. Zaslavsky, Phys. Rev. E 64 (2001) 036221.
[11] A. Iomin, Yu. Bliokh, Comm. Non. Sci. Num. Simul. 8 (2003) 389.
[12] D.G. Ladeira, J.K.L. da Silva, J. Phys. A: Math. Theor. 40 (2007) 11467.
[13] M.V. Berry, Eur. J. Phys. 2 (1981) 91.
[14] M. Robnik, J. Phys. A: Math. Gen. 16 (1983) 3971.
[15] L.A. Bunimovich, Comm. Math. Phys. 65 (1979) 295.
[16] J.E. Howard, A.J. Lichtenberg, M.A. Lieberman, R.H. Cohen, Physica D 20 (1986) 259.
[17] F.R.N. Kock, F. Lenz, C. Petri, F.K. Diakonos, P. Schmelcher, Phys. Rev. E 78 (2008) 056204.
[18] D.F.M. Oliveira, E.D. Leonel, Commun. Nonlinear Sci. Numer. Simul. 15 (2010) 1092.
[19] R. Venegeroles, Phys. Rev. Lett. 101 (2008) 054102.
[20] E.D. Leonel, P.V.E. McClintock, Chaos 15 (2005) 033701.
[21] E. Fermi, Phys. Rev. 75 (1949) 1169.
[22] A.J. Lichtenberg, M.A. Lieberman, R.H. Cohen, Physica D 1 (1980) 291.
[23] E.D. Leonel, M.R. Silva, J Phys. A: Math. Theo. 41 (2008) 015104.
[24] R.K. Pathria, Statistical Mechanics, Elsevier, Burlington, 2008.
[25] G.A. Luna-Acosta, G. Orellana-Rivadeneyra, A. Mendoza-Galván, C. Jung, Chaos Solitons Fractals 12 (2001) 349.
[26] R.C. Hilborn, Chaos and Nonlinear Dynamics, Oxford University Press, 1994.
[27] J.-P Eckmann, D. Ruelle, Rev. Mod. Phys. 57 (1985) 617.
[28] E.D. Leonel, J. Kamphorst Leal da Silva, Phys. A 323 (2003) 181.
[29] E.D. Leonel, J.A. de Oliveira, F. Saif, J. Phys. A 44 (2011) 302001.
[30] E.D. Leonel, P.V.E. McClintock, J.K.L. da Silva, Phys. Rev. Lett. 93 (2004) 014101.
[31] J.A. de Oliveira, R.A. Bizão, Edson D. Leonel, Phys. Rev. E 81 (2010) 046212.